International Journal of Geosciences, 2016, 7, 873-883
Published Online July 2016 in SciRes. http://www.scirp.org/journal/ijg
http://dx.doi.org/10.4236/ijg.2016.77064

Raman and FTIR Spectroscopic Evaluation of Clay Minerals and Estimation of Metal Contaminations in Natural Deposition of Surface Sediments from Brahmaputra River

Bhaskar J. Saikia[1], G. Parthasarathy[2], R. R. Borah[3], R. Borthakur[3,4]

[1]Department of Physics, Anandaram Dhekial Phookan College, Nagaon, India
[2]National Geophysical Research Institute (CSIR-NGRI), Hyderabad, India
[3]Department of Physics, Nowgong College, Nagaon, India
[4]Department of Physics, Assam Down Town University, Guwahati, India
Email: vaskar_r@rediffmail.com

Received 24 May 2016; accepted 5 July 2016; published 8 July 2016

Abstract

This study demonstrates the compositional and structural analysis of surface sediments in natural depositional environment of the Brahmaputra River using X-ray fluorescence, Raman spectroscopic and Fourier transform infrared spectroscopic techniques. The main peaks in the Raman and infrared spectra reflected Al-OH, Al-O and Si-O functional groups in high frequency stretching and low frequency bending modes. The Raman and infrared spectra reveals the nature of clay (kaolinite) associated with quartz. The infrared spectra are indicative to the weathered metamorphic origin of the silicate minerals. The relative distributions of the contaminations in the sediment are: Si > Al > Fe > Mg > Ca > K > Ti > Mn > Cr >Ni > Zn > Cu > Co. The metal contaminations in the sediments are investigated by calculating the enrichment factor, contamination factor, geo-accumulation index and pollution load index. The relative distributions of the contamination among the samples are: Cu > Si > Mn > Mg > Ni > Cr > Ti > Al > Co > Pb > K > Ca > Zn. The investigating factors suggest the significant contamination in the sediment is due to Cu. The strong positive correlation among Al, Fe, Mg and K suggests association of sediments with clay. The elemental correlation is indicative to the metamorphosed pyrophanite ($MnTiO_3$) deposition.

Keywords

Raman Spectroscopy, Sediment, Clay, Metals, Pollution, Brahmaputra River

How to cite this paper: Saikia, B.J., Parthasarathy, G., Borah, R.R. and Borthakur, R. (2016) Raman and FTIR Spectroscopic Evaluation of Clay Minerals and Estimation of Metal Contaminations in Natural Deposition of Surface Sediments from Brahmaputra River. *International Journal of Geosciences*, **7**, 873-883. http://dx.doi.org/10.4236/ijg.2016.77064

1. Introduction

Geochemical studies of sediments are helpful in understanding the different sediment sources, element distribution pattern and evaluating the environmental conditions existing in an area. The mineralogical properties of sediments reflect the geological history of transport and sorting process. The dissolved chemical load and sediment flux of the Brahmaputra river has significantly higher rates of physical and chemical weathering than other large Himalayan catchments [1]-[7]. In total, the Brahmaputra carries over 73 million tons of dissolved material annually, which accounts for approximately 4% of the total dissolved flux to the oceans [7]. The focus on mineralogical, geochemical and geophysical studies and chemical composition of sediments of many Indian rivers were done by many authors [8]-[18]. As river sediments act as both source and sink for heavy metals therefore contaminants may eventually pass through the food chain and result in a wide range of adverse environmental effects. The estimation of silicate distribution in sediments is important because the total CO_2 consumption by silicate weathering can be approximated by the total molar charge equivalents of all cations generated by silicate weathering. In many weathering environment, the chemical weathering of silicate minerals results in the formation of secondary clays. The heavy metal contaminations and silicate mineral distribution in sediments due to weathering of the Brahmaputra river tributaries have been discussed elsewhere by Saikia *et al.* [19] [21]. This spectroscopic study is conducted to evaluate the concentration of clay and metals due to the natural and anthropogenic activities of the Brahmaputra river, which helps to assess the ecotoxic potential of the river sediments.

2. Experimental Methods

The surface sediment samples were collected from six locations viz. Sadiya (27˚49´33˝N, 95˚38´54˝E), Dibrugarh (27˚29´22˝N, 94˚54´58˝E), Dikhomukh (26˚59'20"N, 94˚24'42"N), Dhansirighat (26˚41'17"N, 93˚35'55"E), Kaziranga (26˚45´02˝N, 93˚26´49˝E) and Silghat (26˚36'50"N, 92˚55´58˝E) of the Brahmaputra river (**Figure 1**) and in each locations, five samples were collected at a depth 10 to 30 cm. The sample sites Sadiya, Dibrugarh, Dikhomukh Dhansirighat, Kaziranga and Silghat are denoted S1, S2, S3, S4 and S5 respectively. To eliminate the possibility of materials of the local origin, special care is taken on the sample collection by collecting about 50 - 100 meters away from the stream. Generally, in these sample collection locations, the sediments have been

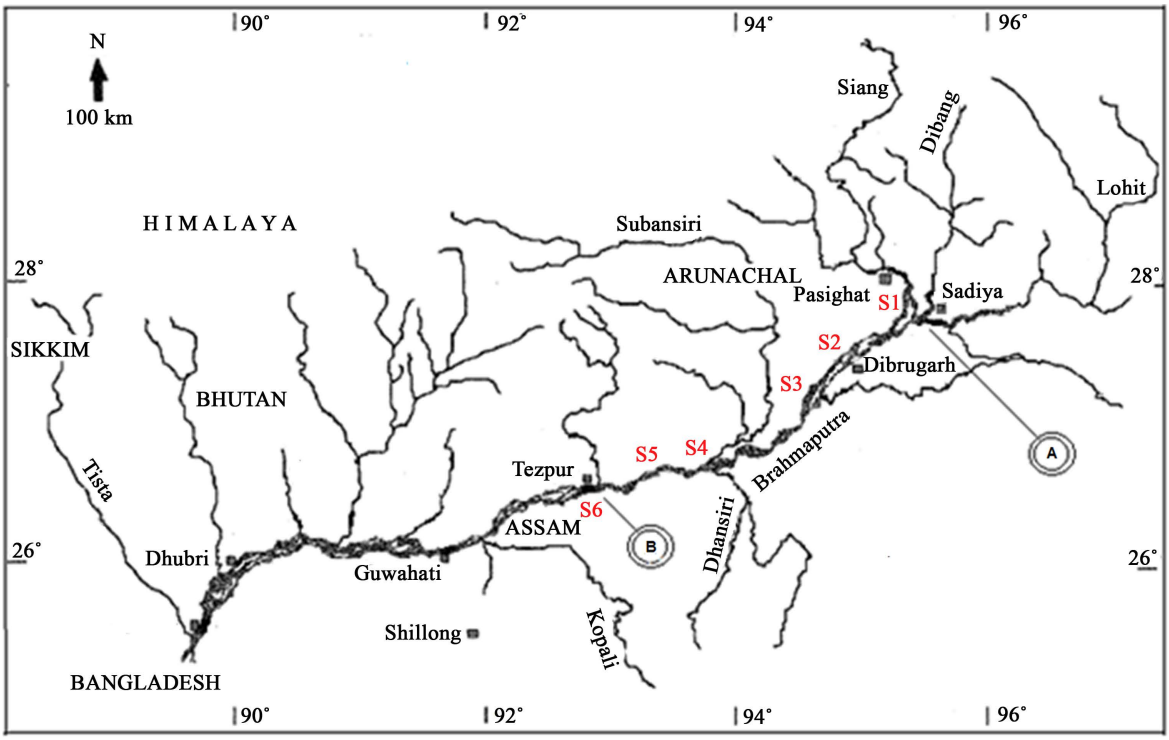

Figure 1. The Brahmaputra River and its tributaries, the sample collection sites are confined between A (Sadiya) and B (Silghat), of length about 350 km of the upper part of the river.

deposited by the river during the summer season or in flood, therefore, all samples are collected in winter the season.

The samples are allowed to dry and the moisture contents are removed by heating the samples at temperature 110˚C for 10 min. The composition of the sediment samples were determined using a Philips MagiX PRO wavelength dispersive X-ray spectrometer with a rhodium anode X-ray tube was used, which may operated at up to 60 kV and current up to 125 mA, at a maximum power level of 4 kW. The precision and accuracy of the data is ±2%, and average values of three replicates were taken for each determination.

The sediment samples were crushed into fine powder for analysis. The powdered sample was homogenized in spectrophotometric grade KBr (1:20) in an agate mortar and was pressed with 3 mm pellets using a hand press. The infrared spectrum was acquired using Perkin-Elmer system 2000 FTIR spectrophotometer with helium–neon laser as the source reference, at a resolution of 4 cm^{-1}. The spectra were taken in transmission mode in the region 400 - 4000 cm^{-1}. The room temperature was 30˚C during the experiment. Raman spectra were collected using a Ar^{+} excitation source having wavelength 488 nm coupled with a Jobin-Yvon Horiba LabRam-HR Micro Raman spectrometer equipped with an Olympus microscope with 10×, 50× and 100× objectives and a motorized x − y stage and using 1800 gr./mm grating in the range from 100 to 4000 cm^{-1}. Spectra were generally collected with counting times ranging between 10 and 60 s.

The enrichment factor (EF), contamination factor (CF), index of geo-accumulation (I_{geo}) and pollution load index (PLI) of the study sediments samples are ascertain by using the standard methods discussed elsewhere [19].

3. Results and Discussions

The Raman spectra of the samples and spectral positions are tabulated in the **Figure 2** and **Table 1** respectively. The observed intense peaks between 100 to 200 cm^{-1} of the Raman spectra demonstrates the presence of clay minerals. The intense peaks at 144 and 123 cm^{-1} of the samples (S3 and S4) demonstrates the presence of kaoli-

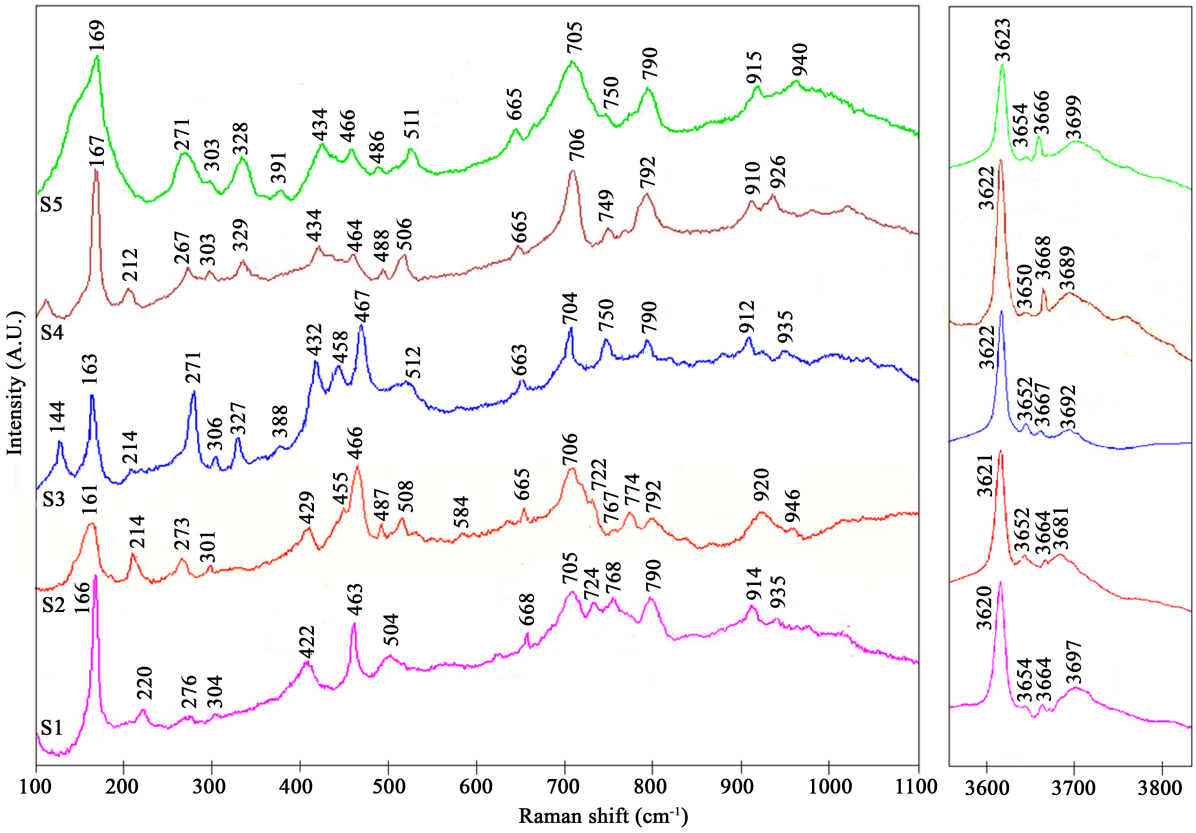

Figure 2. Raman spectra of the sediment samples of the Brahmaputra River.

Table 1. Comparative peak positions (in cm^{-1}) of Raman and infrared spectra with possible assignments and chemical phases.

Raman					Infrared					Assignments	Chemical Phases
S1	S2	S3	S4	S5	S1	S2	S3	S4	S5		
-	-	-	123	-	-	-	-	-	-	O-Si-O symmetric bend	Dickite
-	-	144	-	-	-	-	-	-	-	O-Al-O symmetric bend	Kaolin
166	161	163	167	169	-	-	-	-	-	-	Anatase
220	214	214	212	-	-	-	-	-	-	Fe-O symmetric stretch	Hematite
276	273	271	267	271	-	-	-	-	-	Al-OH; OH + K-O translation	
304	301	306	303	303	-	-	-	-	-	Fe-O symmetric bend	Magnetite
-	-	327	329	328	-	-	-	-	-	O-H-O bend	Kaolin
-	-	388	-	391	-	-	-	-	-	Fe-O-Fe/ -OH symmetric stretch	Goethite
422	429	432	434	434	-	-	-	-	-	Ti-O bend	Rutile
-	-	-	-	-	442	445	440	444	439	SiO_4 symmetric stretch	Kaolin
-	455	458	-	-	-	-	-	-	-	SiO_4 symmetric stretch	
463	466	467	464	466	469	467	-	468	468	Si-O-Si bending	Quartz/Illite
-	487	-	488	486	-	-	470	-	-	-	Kaolin/Geikielite
504	508	512	506	511	-	-	-	-	-	Al-O-Si bend	Feldspar (albite)
-	584	-	-	-	538	536	540	538	541	Si-O-Al deformation	Kaolin/Hematite
-	-	-	-	-	-	641	-	647	649	Si-O-Si bending	Feldspar
668	665	663	665	665	-	-	-	-	-	Fe-O symmetric stretch	Magnetite
-	-	-	-	-	694	694	696	693	696	Si-O	Quartz
705	706	704	706	705	-	-	-	-	-	A1-OH vibrations	Illite
724	722	-	-	-	722	727	724	724	723	O-H bend; Al-O-Si stretch	Kaolin/Feldspar/ Geikielite
768	767	750	749	750	751	-	-	-	-	Al-O-Si stretch	Kaolin
-	774	-	-	-	779	780	777	776	778	Si-O	Quartz
790	792	790	792	790	-	-	-	-	-	Al-O-Si bend	Illite/Kaolin
-	-	-	-	-	799	795	797	794	798	Si-O bend	Quartz/Kaolin
-	-	-	-	-	850	-	839	-	847	Al-O-H stretch	Illite/Montmor
914	920	912	910	915	918	916	920	918	917	Al-OH deformation	Kaolin/Montmor
935	946	935	926	940	939	940	938	942	938	Al-OH deformation	
-	-	-	-	-	1016	1018	1015	1014	1018	Si-O stretching	
-	-	-	-	-	1042	1039	1041	1040	1040	Si-O stretching	Kaolin
-	-	-	-	-	1101	1104	1102	1102	1105	-	
-	-	-	-	-	1118	1120	1117	1118	1116	Si-O stretching	
-	-	-	-	-	1475	1470	-	-	1470	-	Calcium oxalate
-	-	-	-	-	1510	-	1516	1521	-	-	Carbonates
-	-	-	-	-	1620	-	1614	-	-	-	Pyrophanite
-	-	-	-	-	2842	2840	2841	2842	2842	C-H antisymmetric stretching	Organic material
-	-	-	-	-	-	-	2926	2924	2926	C-H symmetric stretching	Organic material
-	-	-	-	-	2954	2956	-	-	-	C-H symmetric stretching	Organic material
3620	3621	3622	3622	3623	3620	3622	3622	3620	3621	*v*4 Stretch inner OH	Kaolin/Illite/ Montmor
3654	3652	3652	3650	3654	3654	3650	3652	3652	3654	*v*3 Stretch inner surface OH	Kaolin
3664	3664	3667	3666	3666	3665	3668	3666	3663	3667	*v*2	
3697	3681	3692	3689	3699	3696	3692	3694	3697	3692	*v*1 Stretch inner surface OH	Kaolin

nite, because in general, the kaolinite minerals are characterized by very intense bands around 143 cm^{-1} [21]-[23]. The bands in this region are attributed to the symmetric bending modes of the O-Si-O and O-A1-O groups. The observed frequency at 144 cm^{-1} is attributed to the $v2(E)$ mode of the AlO_6 octahedron and the frequency at 123 cm^{-1} is attributed to the out of plane vibration of the Si_2O_5. The other bands in between 161 - 169 cm^{-1} are attributed to Raman active $E_g(v_2)$ vibration. The peaks around 161 - 169 cm^{-1} are also characteristic to anatase. The observed bands in between 212 - 220 cm^{-1} and 267 - 276 cm^{-1} are attributed to the vibrational modes $B_2(v_3)$ and $A_l(v_1)$ respectively. The bend around 212 - 220 cm^{-1} arises due to Fe-O (Hematite). Magnetite shows its main Raman peak near 667 cm^{-1}, and is distinguishable from other Fe-oxides of structure, such as chromite, spinel, gahnite and franklinite. The peaks in the range 663 - 668 cm^{-1} (A_{1g}) of all samples are attributed to the existence of magnetite. The other peaks at 301 - 306 cm^{-1} (E_g) of all spectra are indicative to magnetite in the samples. The peaks at 422 - 434 $cm^{-1}$of all spectra are indicative to rutile in the samples. The peaks at 327 - 329 cm^{-1} and 388 - 391 cm^{-1} in the spectra of the samples S3, S4 and S5 correspond to the $v2(E)$ mode of the SiO_4 tetrahedron. The Si-O-Si stretching vibration is observed between 637-645 cm^{-1} in the samples S1 and S2. The band in the region 749 - 751 cm^{-1} is related to the stretching vibration of Si-O bonds. The spectral region 455 - 467 cm^{-1} and 790 - 792 cm^{-1} are observed in all samples and these bends are assigned to quartz. The Raman peaks due to feldspar is observed in between 504 - 512 cm^{-1}. The peak at 511 cm^{-1} is indicative of albite. The relative intensities of the bends in the region 464 and 504 cm^{-1} is indicative to the presence of various amounts of moganite intergrowth with the dominant quartz in all the studied samples [24] [25]. The peak observed in sample S3 at 388 cm^{-1} and S5 at 391 $cm^{-1}$are very nearer to the main peak of goethite occurs at 386 cm^{-1} which suggestive to presence of goethite in the sample. The geikielite ($MgTiO_3$) has a characteristic Raman peaks found at around 720 cm^{-1} and 490 cm^{-1}. A weak band at 722 - 724 cm^{-1} and 486 - 488 cm^{-1} is observed in the spectra which indicate the presence of geikielite in the samples. Generally, the montmorillonite exhibits a peak near 705 cm^{-1} and it can be assigned to Si-O-Si vibration. All observed samples exhibit the peak 704 - 706 cm^{-1} in this region. The observed bends in between 910 - 920 cm^{-1} and 926 - 946 cm^{-1} reveals the bending vibrations of the inner hydroxyl and plain bending vibrations of the surface hydroxyls of kaolinite respectively [26].

The infrared spectra of the studied samples represented in **Figure 3** and the spectral positions are tabulated in **Table 1**. The infrared spectra have shown bands between 1200 - 450 cm^{-1} confirms the existence of quartz one

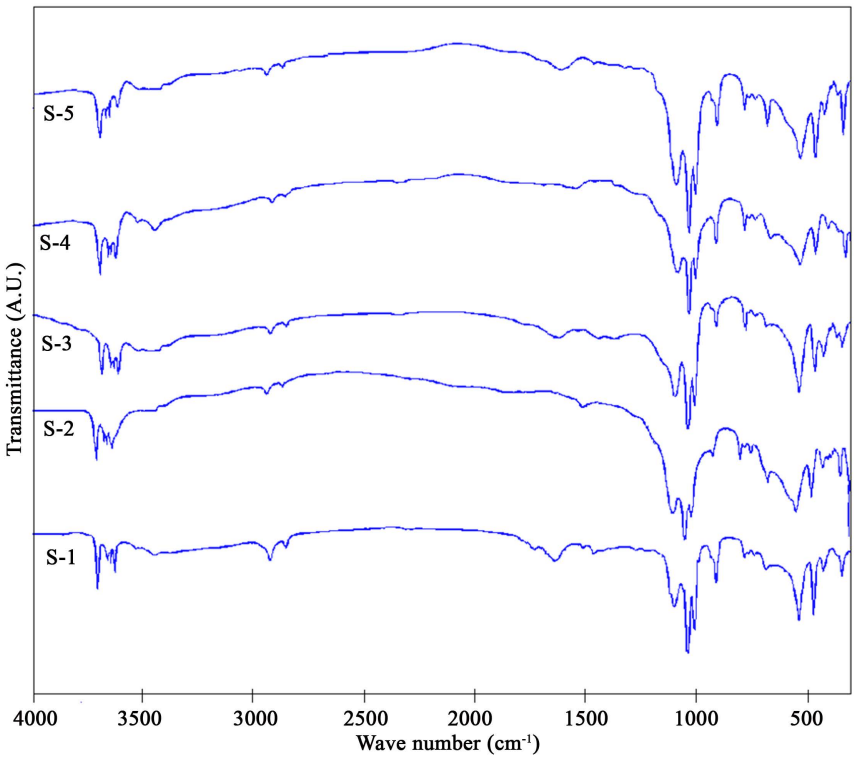

Figure 3. Infrared spectra of the sediment samples of the Brahmaputra River.

of the non clay mineral and invariably present in all samples. The presence of quartz in the samples can be explained by Si-O asymmetrical bending vibrations, Si-O symmetrical bending vibrations, Si-O symmetrical stretching vibrations at around 464 cm^{-1}, 694 cm^{-1} and 778 cm^{-1} respectively. The observed doublet at 914 and 936 cm^{-1} can also be recognized by kaolinite. The infrared peak corresponding to the range 536 - 541 cm^{-1} is arising due to Si-O asymmetrical bending vibrations and 641 - 649 cm^{-1} is arising due to Al-O-coordination vibrations and these peaks are indicative to the presence of orthoclase feldspar [27] [28]. In the infrared spectra, the observed band at 777 - 780 cm^{-1} is arises due to Si–O symmetrical stretching vibration ($v1$), the band at 693 - 696 cm^{-1} is arise due to Si-O symmetrical bending vibration ($v2$), and the peaks around 468 cm^{-1} is arise due to Si–O asymmetrical bending vibration ($v4$) are indicative to quartz. The Si-O symmetrical bending vibrational peak at 695 cm^{-1} of the octahedral site symmetry is unique to the crystalline materials. All infrared spectra reveals peak at this range, therefore crystalline quartz particles present in the observed samples [28]-[30]. The infrared spectra reveals bands at 1014 - 1018 cm^{-1} are close to the SiO deformation band obtained for kaolinite. The absorption band at 1116 - 1120 cm^{-1} is identical to the Si-O normal to the plane stretching. The observed bands in the range 916 - 920 cm^{-1} are assigned to (Al-Al-OH) deformation respectively. The peaks around 920 cm^{-1} are attributed to presence of illite [26] [31]. With the view of Keller and Pickett, 1949, the observed absorption peaks at 1615 - 1620 cm^{-1} in some sites indicate the presence of quartz in river sediments are weathered from metamorphic origin [32]. The infrared peak positions at 1614 and 1620cm^{-1} observed in the sample S3 and S1 respectively have good agreement with the observation on the quartz mineral obtained by Ramasamy *et al.*, and Saikia *et al.* [19] [20] [33].

The doubly degenerate symmetric stretch ($v3$) at the region 1510 - 1521 $cm^{-1}$of the infrared spectra are indicative to carbonates. All infrared spectra exhibits weak absorption bands at 2840 - 2842 cm^{-1} and 2924 - 2956 cm^{-1} arises due to symmetric and asymmetric stretching of CH group which suggest the presence of organic carbon in the studied samples [34] [35]. The OH stretching modes of vibrations in between 3600 to 3800 cm^{-1} are observed in all samples. Generally four bands were found in this region at around 3620, 3649, 3664 and 3686 cm^{-1}. These bands were arises due to the $v4$, $v3$, $v2$ and $v1$ stretching modes of vibrations. The comparative band positions of infrared and Raman are presented in the **Table 1**. The observed band positions in this region are similar to that of the band found for kaolinite. The variation or position shift of the OH stretching modes indicates the disorder nature of kaolinite in the samples. The frequency vibrations 3681 - 3699 cm^{-1} ($v1$), 3664 - 3667 cm^{-1} ($v2$) and 3650 - 3654 cm^{-1} ($v3$) are due to the three inner surface hydroxyls whereas the vibrations at 3620 - 3623 cm^{-1} ($v1$) is due to the inner hydroxyl [36]. The $v1$ band observed in infrared spectra around 3620 cm^{-1} has been assigned to the inner hydroxyl of kaolinite by many authors [37]-[40]. Generally the bands $v1$, $v2$ and $v3$ are arises due to the coupled antisymmetric vibrations, symmetric vibrations and due to symmetry reduction from an inner surface hydroxyl respectively [23] [41] [42].

The oxide composition of the sediments in sample site S1 to S5 is estimated as: SiO_2 (66.74 ± 2.07 wt%), Al_2O_3 (22.99 ± 2.14 wt%), Fe_2O_3 (2.04 ± 0.74 wt%), MgO (2.88 ± 1.25 wt%), MnO (0.09 ± 0.08 wt%), CaO (0.72 ± 0.17 wt%), Na_2O (0.95 ± 0.20 wt%), K_2O (1.07 ± 0.66 wt%) and TiO_2 (0.94 ± 0.13 wt%). The metal concentrations in the sediment samples of Brahmaputra river are presented in the **Table 2**. The concentrations of the elements are compared with different reference data and results of the previous worker Subramanian *et al.* [9] [10]. Average concentrations of Al, Fe, Ni, Pb, Ti, Zn, K, Ca, Co and Cr are found to be below of their respective reference values. Whereas the concentrations of Si, Mg, Mn and Cu has greater average values than the respective reference values. The concentration of K, Ca and Cr are slightly below the results of the previous worker Subramanian *et al.* [9] [10]. The world surface rock represents the average lithology subjected to weathering in the hydrosphere. The world surface rock average prescribed by Martin and Meybeck is used as background value for investigation of enrichment factor (EF), contamination factor (CF), index of geo-accumulation (I_{geo}) and pollution load index (PLI) of the sediments samples [43]. The average concentrations of all observed elements except Si and Mg have less than the world surface rock average as background level. The enrichment factor, contamination factor and geo-accumulation index of the study samples were depicted in **Table 3**.

Titanite is a common accessory mineral in sediments from the igneous and metamorphic origin and has affects low due to weathering. The strong positive correlation of Ti with Ca (0.96) suggests the presence of titanite minerals in the samples. The positive correlation of Ti with Mn (0.94) suggests the presence of pyrophanite ($MnTiO_3$). The presence of $MnTiO_3$ in the tributaries of Brahmaputra has been already reported by Saikia *et al.* [19] [20]. The elements Pb and Fe expressed a strong positive correlation with Zn, Co and Mg, Mn, Ti, K, Ca respectively at 0.05 level. The other elements such as Al has strong positive correlation with Fe, Mg, Mn, Ti, K

Table 2. Comparative concentation of elements in Brahmaputra river sediments (in ppm).

Elements	Concentration of elements for site S1 to S5			BBS*	IRSA*	WRA*	WSRA*	WSA*
	Min	Max	average ± standard deviation					
Si	302,336	303100	302,716 ± 346.55	-	-	285,000	275,000	330,000
Al	56,914	59155	57,832 ± 943.52	56,000	-	94,000	69,300	71,000
Fe	28,941	35520	31,030.40 ± 2663.76	29,000	29000	48,000	35,900	40,000
Mg	16,150	17311	16,716.60 ± 518.88	16,500	-	11,800	16,400	5000
Mn	700	850	780 ± 57.01	600	605	1050	720	1000
Cu	29	44	37.20 ± 6.22	17	28	100	32	30
Ni	33	67	48.20 ± 13.37	47	37	90	49	50
Pb	6.77	11.63	9.61 ± 2.03	-	-	150	16	12
Ti	2700	3800	3300 ± 418.33	3100	-	4160	3800	5000
Zn	43	59	51.80 ± 6.42	47	16	350	129	90
K	9000	13000	11,600 ± 1673.32	12,000	-	14,200	24,400	14,000
Ca	17,400	19500	18,660 ± 844.39	19,300	-	21,500	45,000	15,000
Co	8.71	10.53	9.44 ± 0.76	-	-	20	13	8
Cr	87.51	96.38	90.32 ± 3.48	100	87	100	97	70

*Brahmaputra basin sediment (BBS) [9]; Indian river sediment average (IRSA) [10]; Worlds river average (WRA); Worlds sur face rock average(WSRA) [43]; Worlds soil average (WSA) [49].

Table 3. Pearson's correlation coefficient between metal elements of the Brahmaputra river sediments ($p < 0.05$).

	Si	Al	Fe	Mg	Mn	Cu	Ni	Pb	Ti	Zn	K	Ca	Co	Cr
Si	1.00													
Al	**1.00**	1.00												
Fe	**0.98**	**0.98**	1.00											
Mg	**1.00**	**1.00**	**0.98**	1.00										
Mn	**0.98**	**0.98**	**0.99**	**0.98**	1.00									
Cu	−0.98	−0.98	−0.93	−0.97	−0.93	1.00								
Ni	−0.87	−0.88	−0.79	−0.88	−0.83	0.90	1.00							
Pb	−1.00	−1.00	−0.98	−0.99	−0.98	**0.98**	0.88	1.00						
Ti	**0.96**	**0.97**	0.91	**0.97**	0.94	−0.93	−0.92	−0.95	1.00					
Zn	−0.96	−0.96	−0.91	−0.96	−0.91	**1.00**	0.89	**0.97**	−0.91	1.00				
K	**0.95**	**0.95**	**0.97**	**0.95**	0.93	−0.91	−0.70	−0.94	0.88	−0.91	1.00			
Ca	**0.99**	**0.99**	**0.97**	**0.99**	**0.98**	−0.98	−0.91	−1.00	**0.96**	−0.97	0.93	1.00		
Co	−1.00	−1.00	−0.98	−1.00	−0.98	**0.98**	0.88	1.00	−0.96	**0.96**	−0.95	−1.00	1.00	
Cr	−0.82	−0.81	−0.83	−0.83	−0.87	0.71	0.66	0.81	−0.84	0.67	−0.77	−0.78	0.81	1.00

and Ca; Cu has strong positive correlation with Ni, Pb, Zn and Co; Ti has strong positive correlation with Ca; Zn has strong positive correlation with Co at this level of significance (**Table 3**). The strong correlation indicates that these elements have common sources. The strong positive correlation among Al, Fe, Mg and K suggests their association with clay.

The possible anthropogenic impact in the sediment is ascertain by enrichment factor (EF) based on the standardization of the analyzed element against a reference element. The element which has low occurrence variability is considered as a reference element. Generally geochemical normalization of the heavy metals data to a conservative element, such as Al, Si and Fe is employed. In this study Fe is considered as reference element of normalization because natural sources (1.5%) vastly dominate its input [14] [15] [44]. The calculated enrichment of different elements is presented in **Table 4**. According to Mmolawa *et al.*, the categories of enrichment factor are deficiency to minimal enrichment (EF < 2); moderate enrichment (2 ≤ EF < 5); significant enrichment (5 ≤ EF < 20); very high enrichment (20 ≤ EF < 40) and extremely high enrichment (EF ≥ 40) [45]. **Table 4** displays the enrichment factor of the all observed elements has a value in the range of minimal enrichment. The enrichment of Cu is relatively higher than other elements.

The index of geo-accumulation (I_{geo}) is characterized according to the Muller seven grades or classes profile of the geo-accumulation index *i.e.* the value of sediment quality is considered as unpolluted (I_{geo} is ≤0, class 0); from unpolluted to moderately polluted (I_{geo} is 0 - 1, class 1); moderately polluted (I_{geo} is 1 - 2, class 2); from moderately to strongly polluted (I_{geo} is 2 - 3, class 3); Strongly polluted (I_{geo} is 3 - 4, class 4); from strongly to extremely polluted (I_{geo} is 4 - 5, class 5) and Extremely polluted (I_{geo} is >6, class 6) [46]. The calculated Igeo values for all elements were negative (**Table 4**). Therefore, according to Muller's classification, Brahmaputra river sediments were unpolluted (class 0). The total index of geo-accumulation (I_{tot}) is defined as the sum of I_{geo} for all trace elements obtain from the site [47]. The total index of geo-accumulation for the Brahmaputra river sediment is −3.818 ± 0.593.

The metal contamination level of the sediment is ascertained by the level of contamination proposed by Hakanson [48]. According to Hakanson the classifications are: low contamination (CF < 1); moderate contamination (1 ≤ CF < 3); considerable contamination (3 ≤ CF < 6) and very high contamination (CF > 6). All elements except Si, Mg, Mn and Cu has low contamination value (**Table 4**). The sediment is moderately contaminated due to Si, Mg, Mn and Cu. The relative distributions of the contamination factor among the samples are: Cu > Si > Mn > Mg > Ni > Cr > Ti > Al > Co > Pb > K > Ca > Zn. The value of mean pollution load index of the sediments is estimated as 0.771 ± 0.046. The mean pollution load indexes of all sites suggest no overall pollution and are almost identical to the mean pollution load of the Subansiri river [19].

Table 4. Enrichment factor, Contamination factor and Geo-accumulation index of the Brahmaputra river sediments.

Elements (ppm)	Sample sites S1 to S5		
	Enrichment Factor (EF) average ± SD	Contamination Factor (CF) average ± SD	Geo-accumulation Index (I_{geo}) average ± SD
Si	1.281 ± 0.101	1.101 ± 0.001	−0.134 ± 0.001
Al	0.971 ± 0.082	0.835 ± 0.014	−0.255 ± 0.007
Mg	1.186 ± 0.108	1.019 ± 0.032	−0.168 ± 0.013
Mn	1.256 ± 0.077	1.083 ± 0.079	−0.142 ± 0.032
Cu	1.342 ± 0.173	1.163 ± 0.194	−0.116 ± 0.075
Ni	1.128 ± 0.241	0.984 ± 0.273	−0.197 ± 0.111
Pb	0.698 ± 0.152	0.601 ± 0.127	−0.406 ± 0.096
Ti	1.015 ± 0.175	0.868 ± 0.110	−0.240 ± 0.057
Zn	0.465 ± 0.043	0.402 ± 0.050	−0.575 ± 0.055
K	0.550 ± 0.070	0.475 ± 0.069	−0.503 ± 0.067
Ca	0.483 ± 0.051	0.415 ± 0.019	−0.559 ± 0.020
Co	0.843 ± 0.079	0.726 ± 0.059	−0.316 ± 0.035
Cr	1.084 ± 0.106	0.931 ± 0.036	−0.207 ± 0.016

4. Conclusion

Raman and infrared spectra indicate the most abundant constituents of the sediments are crystalline quartz with clay minerals which is identical to the compositional results. All infrared spectra of the studied samples exhibit peaks near 695 cm^{-1} which indicative to the presence of micro-crystalline quartz particles in the sediment samples. The identical clays are kaolinite, montmorillonite and illite, The other constituents present in the sediment are titanite, hematite, magnetite, pargasite, moganite, geikielite, feldspars (orthoclase, albite), carbonates and organic compounds. The presence of infrared absorption peaks in between 1614 - 1620 cm^{-1} is indicative to the weathered metamorphic origin of the silicate minerals. The observed positive correlation between Ti and Mn is indicative to the presence of pyrophanite ($MnTiO_3$) mineral from the metamorphosed manganese deposition in the adjoin areas. The strong positive correlation among Al, Fe, Mg and K suggests their association with clay. The Raman peaks (at 722 - 724 cm^{-1} and 486 - 488 cm^{-1}) and positive correlation of Ti and Mg (0.97) are indicative to presence of geikielite ($MgTiO_3$) in the samples. The enrichment factor and contamination factor has a minimal value. The mean pollution load indexes of all sites suggest no overall pollution. The overall sediment is moderately contaminated due to Si, Mg, Mn and Cu. The relative distributions of the contamination factor among the samples are: Cu > Si > Mn > Mg > Ni > Cr > Ti > Al > Co > Pb > K > Ca > Zn. The negative value of geo-accumulation index indicates that the mean concentrations of metals Brahmaputra river sediments are lower than world surface rock average.

Acknowledgements

We thank Directors, National Geophysical Research Institute (NGRI-CSIR), Hyderabad, Indian Institute of Technology, Guwahati (IITG) and North East Institute of Science and Technology (NEIST-CSIR), Jorhat for their cooperation during this work. We also thank Dr. J.R. Chetia, Dibrugarh University, Dibrugarh, for his assistance in the FTIR analysis.

References

[1] Sarin, M.M., Krishnaswami, S., Dilli, K., Somayajulu, B.L.K. and Moore, W.S. (1989) Major Ion Chemistry of the Ganga-Brahmaputra River System: Weathering Processes and Fluxes to the Bay of Bengal. *Geochimica et Cosmochimica Acta*, **53**, 997-1009. http://dx.doi.org/10.1016/0016-7037(89)90205-6

[2] Harris, N., Bickle, M.J., Chapman, H., Fairchild, I. and Bunbury, J. (1998) The Significance of Himalayan Rivers for Silicate Weathering Rates: Evidence from the Bhote Kosi Tributary. *Chemical Geology*, **144**, 205-220. http://dx.doi.org/10.1016/S0009-2541(97)00132-0

[3] Galy, A. and France-Lanord, C. (1999) Weathering Processes in the Ganges-Brahmaputra Basin and the Riverine Alkalinity Budget. *Chemical Geology*, **159**, 31-60. http://dx.doi.org/10.1016/S0009-2541(99)00033-9

[4] Galy, A. and France-Lanord, C. (2001) Higher Erosion Rates in the Himalaya: Geochemical Constraints on Riverine Fluxes. *Geology*, **29**, 23-26. http://dx.doi.org/10.1130/0091-7613(2001)029<0023:HERITH>2.0.CO;2

[5] Dalai, T.K., Krishnaswami, S. and Sarin, M.M. (2002) Major Ion Chemistry in the Headwaters of the Yamuna River System: Chemical Weathering, Its Temperature Dependence and CO_2 Consumption in the Himalaya. *Geochimica et Cosmochimica Acta*, **66**, 3397-3416. http://dx.doi.org/10.1016/S0016-7037(02)00937-7

[6] Singh, S.K. and France-Lanord, C. (2002) Tracing the Distribution of Erosion in the Brahmaputra Watershed from Isotopic Compositions of Stream Sediments. *Earth and Planetary Science Letters*, **202**, 645-662. http://dx.doi.org/10.1016/S0012-821X(02)00822-1

[7] Singh, S., Sarin, M.M. and France-Lanord, C. (2005) Chemical Erosion in the Eastern Himalaya: Major Ion Composition of the Brahmaputra and d13C of Dissolved Inorganic Carbon. *Geochimica et Cosmochimica Acta*, **69**, 3573-3588. http://dx.doi.org/10.1016/j.gca.2005.02.033

[8] Borole, D.V., Sarin, M.M. and Somayajulu, B.L.K. (1982) Composition of Narmada and Tapti Estuarine Particles and Adjacent Arabian Sea Sediments. *Indian Journal of Marine Sciences*, **11**, 51-62.

[9] Subramanian, V., Van't Dack, L. and Grieken, V. (1985) Chemical Composition of River Sediments from the Indian Subcontinent. *Chemical Geology*, **48**, 271-279. http://dx.doi.org/10.1016/0009-2541(85)90052-X

[10] Subramanian, V., Grieken, R.V. and Dack, L.V. (1987) Heavy Metals Distribution in the Sediments of Ganges and Brahmaputra Rivers. *Environmental Geology and Water Sciences*, **9**, 93-103. http://dx.doi.org/10.1007/BF02449940

[11] Seralathan, P. (1987) Trace Element Geochemistry of Modern Deltaic Sediments of the Cauvery River, East Coast of India. *Indian Journal of Marine Sciences*, **16**, 235-239.

[12] Ramesh, R., Subramanian, V. and Van Grieken, R. (1990) Heavy Metal Distribution in Sediments of Krishna River Basin, India. *Environmental Geology and Water Sciences*, **15**, 303-324. http://dx.doi.org/10.1007/BF01706412

[13] Chakrapani, G.J. and Subramanian, V. (1990) Preliminary Studies on the Geochemistry of the Mahanadi River Basin, India. *Chemical Geology*, **70**, 247-266. http://dx.doi.org/10.1016/0009-2541(90)90118-q

[14] Singh, M., Ansari, A.A., Muller, G. and Singh, I.B. (1997) Heavy Metals in Freshly Deposited Sediments of the Gomti River (a Tributary of the Ganga River): Effects of Human Activities. *Environmental Geology*, **29**, 246-252. http://dx.doi.org/10.1007/s002540050123

[15] Kotoky, P., Baruah, J., Baruah, N.K. and Sarma, J.N. (1997) Geoenvironmental Studies of the River Jhanji, Assam. *Journal of Human Ecology*, **6**, 55-67.

[16] Singh, A.K. (1999) Elemental Composition of the Damodar River Sediments—A Tributary of the Lower Ganga, India. *Journal of the Geological Society of India*, **53**, 219-231.

[17] Dekov, V.M., Araújo, F., Van Grieken, R. and Subramanian, V. (1998) Chemical Composition of Sediments and Suspended Matter from the Cauvery and Brahmaputra Rivers (India). *Science of the Total Environment*, **212**, 89-105. http://dx.doi.org/10.1016/S0048-9697(97)00132-0

[18] Braun, J.J., Descloîtres, M., Riotte, J., Fleury, S., Barbiero, L., Boeglin, J., Violette, A., Lacarce, E., Ruiz, L., Sekhar, M., Kumar, M.S.M., Subramanian, S. and Dupré, B. (2009) Regolith Mass Balance Inferred from Combined Mineralogical, Geochemical and Geophysical Studies: Mule Hole Gneissic Watershed, South India. *Geochimica et Cosmochimica Acta*, **73**, 935-961. http://dx.doi.org/10.1016/j.gca.2008.11.013

[19] Saikia, B.J., Goswami, S.R. and Borah, R.R. (2014) Estimation of Heavy Metals Contamination and Silicate Mineral Distributions in Suspended Sediments of Subansiri River. *International Journal of Physical Sciences*, **9**, 475-486.

[20] Saikia, B.J., Goswami, S.R., Borthakur, R., Roy, I.B. and Borah, R.R. (2015) Spectroscopic Characterization and Quantitative Estimation of Natural Weathering of Silicates in Sediments of Dikrong River, India. *Journal of Modern Physics*, **6**, 1631-1641. http://dx.doi.org/10.4236/jmp.2015.611164

[21] Wiewiora, A., Wieckowski, T. and Sokolowska, A. (1979) The Raman Spectra of Kaolinite Sub-Group Minerals and of Pyrophyllite. *Archiwum Mineralogiczne*, **135**, 5-14.

[22] Johnston, C.T., Sposito, G. and Birge, R.R. (1985) Raman Spectroscopic Study of Kaolinite in Aqueous Suspension. *Clays and Clay Minerals*, **33**, 483-489. http://dx.doi.org/10.1346/CCMN.1985.0330602

[23] Michaelian, K.H., Bukka, K. and Permann, D.N.S. (1987) Photoacoustic Infrared Spectra (250 - 10,000 cm^{-1}) of Partially Deuterated Kaolinite. *Canadian Journal of Chemistry*, **65**, 1420-1423. http://dx.doi.org/10.1139/v87-240

[24] Götze, J., Nasdala, L., Kleeberg, R. and Wenzel, M. (1998) Occurrence and Distribution of "Moganite" in Agate/Chalcedony: A Combined Micro-Raman, and Cathodoluminescence Study. *Contributions to Mineralogy and Petrology*, **133**, 96-105. http://dx.doi.org/10.1007/s004100050440

[25] Kingma, K.J. and Hemley, R. (1994) Raman Spectroscopy Study of Microcrystalline Silica. *American Mineralogist*, **79**, 269-273.

[26] Farmer, V.C. (1974) The Infrared Spectra of Minerals. Mineralogical Society, London. http://dx.doi.org/10.1180/mono-4

[27] Saikia, B.J., Parthasarathy, G. and Sarmah, N.C. (2008) Fourier Transform Infrared Spectroscopic Estimation of Crystallinity in SiO_2 Based Rocks. *Bulletin of Materials Science*, **31**, 775-779. http://dx.doi.org/10.1007/s12034-008-0123-0

[28] Saikia, B.J. (2014) Spectroscopic Estimation of Geometrical Structure Elucidation in Natural SiO_2 Crystal. *Journal of Materials Physics and Chemistry*, **2**, 28-33. http://dx.doi.org/10.12691/jmpc-2-2-3

[29] Saikia, B.J. and Parthasarathy, G. (2010) Fourier Transform Infrared Spectroscopic Characterization of Kaolinite from Assam and Meghalaya, Northeastern India. *Journal of Modern Physics*, **1**, 206-210. http://dx.doi.org/10.4236/jmp.2010.14031

[30] Saikia, B.J., Parthasarathy, G. and Borah, R.R. (2015) Distribution of Microcrystalline Quartz in Glassy Fulgurites from Garuamukh and Kimin, India. *Journal of Applied Mathematics and Physics*, **3**, 1343-1351. http://dx.doi.org/10.4236/jamp.2015.310161

[31] Clark, R.N., King, T.V.V., Kiejwa, M., Swayze, G.A. and Verge, N. (1990) High Spectral Resolution Reflectance Spectroscopy of Minerals. *Journal of Geophysical Research*, **95**, 12653-12680. http://dx.doi.org/10.1029/JB095iB08p12653

[32] Keller, W.D. and Pickett, E.E. (1949) Absorption of Infrared Radiation by Powdered Silica Minerals. *American Mineralogist*, **34**, 855-868.

[33] Ramasamy, V., Rajkumar, P. and Ponnusamy, V. (2006) FTIR Spectroscopic Analysis and Mineralogical Characterization of Vellar River Sediments. *Bulletin of Pure & Applied Sciences*, **25**, 49-55.

[34] Saikia, B.J., Parthasarathy, G. and Sarmah, N.C. (2009) Fourier Transform Infrared Spectroscopic Characterization of Dergaon H5 Chondrite: Evidence of Aliphatic Organic Compound. *Nature and Science*, **7**, 45-51.

[35] Saikia, B.J., Parthasarathy, G., Sarmah, N.C. and Baruah, G.D. (2008) Fourier-Transform Infrared Spectroscopic Characterization of Naturally Occurring Glassy Fulgurites. *Bulletin of Materials Science*, **31**, 155-158. http://dx.doi.org/10.1007/s12034-008-0027-z

[36] Johnston, C.T., Agnew, S.E. and Bish, D.L. (1990) Polarised Single Crystal Fourier-Transform Infrared Microscopy of Ouray Dickite and Keokuk Kaolinite. *Clays and Clay Minerals*, **38**, 573-583. http://dx.doi.org/10.1346/CCMN.1990.0380602

[37] Ledoux, R.L. and White, J.L. (1964) Infrared Study of Selective Deuteration of Kaolinite and Halloysite at Room Temperature. *Science*, **145**, 47-49. http://dx.doi.org/10.1126/science.145.3627.47

[38] Wada, K. (1967) A Study of Hydroxyl Groups in Kaolin Minerals Utilising Selective Deuteration and Infrared Spectroscopy. *Clay Minerals*, **7**, 51-61. http://dx.doi.org/10.1180/claymin.1967.007.1.05

[39] White, J.L. (1971) Interpretation of Infrared Spectra of Soil Minerals. *Soil Science*, **112**, 22-31. http://dx.doi.org/10.1097/00010694-197107000-00005

[40] Rouxhet, P.G., Samudacheata, N., Jacobs, H. and Anton, O. (1977) Attribution of the OH stretching Bands of Kaolinite. *Clay Minerals*, **12**, 171-178. http://dx.doi.org/10.1180/claymin.1977.012.02.07

[41] Brindley, G.W., Chih-Chun, K., Harrison, J.L., Lipsiscas, M. and Raythatha, R. (1986) Relation between the Structural Disorder and Other Characteristics of Kaolinites and Dickites. *Clays and Clay Minerals*, **34**, 233-249. http://dx.doi.org/10.1346/CCMN.1986.0340303

[42] Farmer, V.C. and Russell, J.D. (1964) The Infrared Spectra of Layered Silicates. *Spectrochimica Acta*, **20**, 1149-1173. http://dx.doi.org/10.1016/0371-1951(64)80165-X

[43] Martin, J.M. and Meybeck, M. (1979) Elemental Mass-Balance of Material Carried by Major World Rivers. *Marine Chemistry*, **7**, 173-206. http://dx.doi.org/10.1016/0304-4203(79)90039-2

[44] Tippie, V. (1984) An Environmental Characterization of Chesapeake Bay and a Framework for Action. In: Kennedy, V., Ed., *The Estuary as a Filter*, Academic Press, New York, 467-487. http://dx.doi.org/10.1016/B978-0-12-405070-9.50028-1

[45] Mmolawa, K., Likuku, A. and Gaboutloeloe, G. (2011) Assessment of Heavy Metal Pollution in Soils along Roadside Areas in Botswana. *African Journal of Environmental Science and Technology*, **5**, 186-196.

[46] Muller, G. (1969) Index of Geoaccumulation in Sediments of the Rhine River. *GeoJournal*, **2**, 108-118.

[47] Ya, Z.G., Zhou, L.F., Bao, Z.Y., Gao, P. and Sun, X.W. (2007) High Efficiency of Heavy Metal Removal in Mine Water by Limestone. *Chinese Journal of Geochemistry*, **28**, 293-298. http://dx.doi.org/10.1007/s11631-009-0293-5

[48] Hakanson, L. (1980) An Ecological Risk Index for Aquatic Pollution Control. A Sedimentological Approach. *Water Research*, **4**, 975-1001. http://dx.doi.org/10.1016/0043-1354(80)90143-8

[49] Bowen, H.J.M. (1979) Environmental Chemistry of the Elements. Academic Press, New York, 1-320.